JMEPEG (2006) 15:414-421
DOI: 10.1361/105994906X117215

1059-9495/$19.00

Compressive Mica Seals for Solid Oxide Fuel Cells

Yeong-Shyung Chou and Jeffry W. Stevenson

(Submitted January 16, 2006; in revised form May 18, 2006)

Sealing technology is currently considered a top-priority task for planar solid oxide fuel-cell stack development. Compressive mica seals are among the major candidates for sealing materials due to their thermal, chemical, and electrical properties. In this paper, a comprehensive study of mica seals is presented. Two natural micas, muscovite and phlogopite, were investigated in either a monolithic single-crystal sheet form or a paper form composed of discrete mica flakes. A "hybrid" mica seal, developed after identification of the major leak paths in compressive mica seals, demonstrated leak rates that were hundreds to thousands times lower than leak rates for conventional mica seals. The hybrid mica seals were further modified by infiltration with wetting materials; these "infiltrated" micas showed excellent thermal cycle stability with very low leak rates (10^{-3} sccm/cm). The micas were also subjected to studies to evaluate thermal stability in a reducing environment as well as the effect of compressive stresses on leak rates. In addition, long-term open circuit voltage measurements versus thermal cycling showed constant voltages over 1,000 cycles. The comprehensive study clearly demonstrated the potential of compressive mica seals as sealing candidates for solid oxide fuel cells.

Keywords leak rate, mica, open circuit voltage, phlogopite

1. Introduction

The need to develop a robust sealant or sealants for solid oxide fuel cells (SOFC) has been recognized as one of the major tasks for advancing SOFC technology. For planar SOFC stacks, the sealing requirements are quite challenging due to the multiple sealing sections present. Figure 1 shows the schematic of a typical planar SOFC stack with repeating cells: a ceramic positive electrode/electrolyte/negative electrode (PEN) plate, a window frame (metal or ceramic), and an interconnect (metal or ceramic). In general, planar SOFC stacks have up to four different sealing sections: S1 is the seal between the ceramic PEN plate and the metallic (or ceramic) window frame, S2 is the seal between the window frame and the interconnect (metallic or ceramic) plate, S3 is the seal between the ceramic spacer (if required) and the window frame (or the metallic interconnect), and S4 is the seal between the base manifold and the stack. The seals need to provide zero or low leak rates to avoid direct mixing of the fuel and oxidant gases or leakage of fuel gas from the stack. They must demonstrate long-term thermal and chemical stability in the SOFC environment (40,000 h or more). Finally, they must survive multiple thermal cycles (possibly hundreds to thousands of cycles) during lifetime service in stationary or transportation applications. To do so, they have to be able to withstand transient stresses developed during startup or shutdown and residual stresses due to mismatch in thermal expansion of different SOFC stack components. Currently, there are three primary approaches for SOFC seal development: rigid glass (or glass-ceramic and glass fiber composite) seals (Ref 1-5), metallic brazes (Ref 6,7), and compressive seals (Ref 8-12). Among these approaches, compressive mica seals offer a unique advantage in terms of tolerance of mismatch of coefficient of thermal expansion (CTE) of mating materials, whereas the other approaches require closely matched CTEs.

In this paper, a comprehensive study of the compressive mica seals will be presented. In this study, the origin of leaks was first identified for conventional compressive mica seals. A "hybrid" mica seal was then developed and tested using several types of mica. The effect of compressive stresses on seal behavior was examined. The hybrid mica seal was further modified by using "infiltrated" micas. Results of tests evaluating thermal stability, open circuit voltage versus long thermal cycling, and combined aging and thermal-cycling effects will be reported.

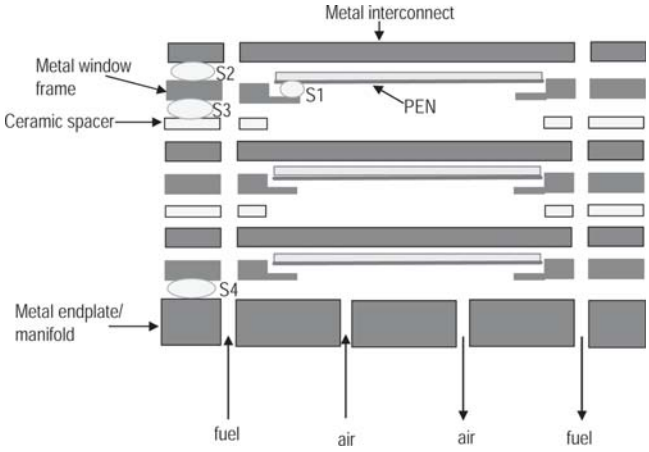

Fig. 1 Multiple sealing sections in a typical planar SOFC stack. S1 is the seal between ceramic PEN plate and the metal window frame, S2 is the seal between the metal frame and the interconnect, S3 is the seal between the ceramic spacer and the metal frame and the interconnect, and S4 is the seal between the manifold and the last cell.

This paper was presented at the ASM Materials Solutions Conference & Show held October 18-21, 2004 in Columbus, OH.

Yeong-Shyung Chou and **Jeffry W. Stevenson,** Materials Division, Pacific Northwest National Laboratory, P.O. Box 999, Richland, WA 99354. Contact e-mail: Yeong-Shyung.Chou@pnl.gov.

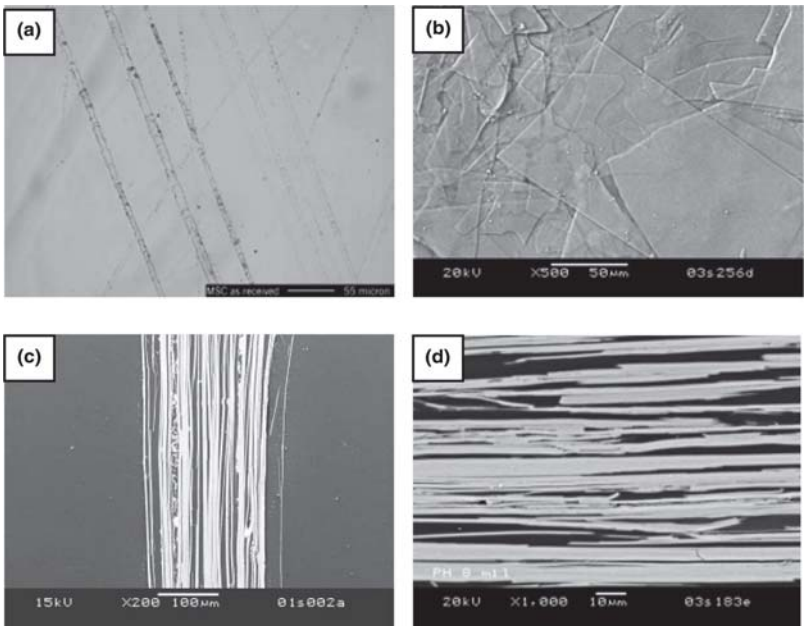

Fig. 2 Micrographs showing the surface morphology of (a) naturally cleaved muscovite single-crystal sheet and (b) phlogopite mica paper. Cross-section views are shown (c) for the naturally cleaved mica sheet and (d) for the phlogopite mica paper.

2. Experimental Procedures

2.1 Materials

Three commercially available micas were investigated in this study. One was a naturally cleaved muscovite single-crystal sheet ~100 μm thick. The other two were muscovite paper and phlogopite paper, each with a thickness of ~100 or ~200 μm. The mica papers were composed of large mica flakes overlapping with each other (~1 mm in diameter; ~10 μm thick) and held together with an organic binder (~3-5 wt.%). Figure 2 shows micrographs of the naturally cleaved muscovite mica sheet (a) and the phlogopite mica paper (b). The naturally cleaved mica was monolithic in nature and had a few surface defects, such as fine scratches. Upon heat treatment at 600-800 °C, the naturally cleaved muscovite mica sheets lost water and cleaved into multiple layers when viewed in cross-section (C) (Ref 9). The cross-section of the phlogopite mica paper (D) shows the overlapping of the mica flakes.

2.2 Leak Testing

Mica samples were cut into 38 mm squares with a 12.7 mm diameter central hole. The mica squares were then pressed between an Inconel tube (outer diameter = 33 mm; inner diameter = 25 mm) and a dense alumina substrate. Some larger mica samples (50 × 50 mm) were also tested, using a 50 × 50 mm Inconel fixture with wall thickness of ~5 mm. The mica samples were tested in the conventional way (i.e., simple mica gasket) as well as in a 'hybrid" design. For hybrid compressive seals, glass interlayers were placed between the Inconel tube/mica and mica/alumina interfaces (Fig. 3). Samples were heated in a clamshell furnace at a heating rate of ~2 °C/min to 800 °C. The load was applied using a universal mechanical tester with a constant load control (Model 5581, Instron, Canton, MA). The experimental setup is shown schematically in Fig. 4. A large known-volume (370 cm^3) reservoir was kept at ambient conditions and connected to the sample via a 3.2 mm Cu tube. By setting up a vacuum in the system (initially as low as ~13.3 Pa), the leak rate was measured by monitoring the pressure change with time. The final pressure was about 2 torr. The pressure gradient across the seal therefore could be considered essentially constant at 101.4 kPa. Assuming the ideal gas law, the leak rate (L) was calculated by the equation:

$$L = \frac{\Delta n}{\Delta t} = \frac{n_f - n_i}{t_f - t_i} = \frac{(p_f - p_i)V}{RT(t_f - t_i)}$$

where n is the moles of the gas, T is the temperature, V is the reservoir volume, R is the gas constant, t is the time, and p is the pressure. Subscripts f and i represent the final and the initial conditions, respectively. The calculated leak rate (L, in standard cubic centimeters per minute at STP, sccm) was further normalized with respect to the outer leak length (10.5 cm) of the Inconel tube and to a pressure gradient of 14 kPa by the equation:

$$\bar{L} = \frac{L \times 2}{10.5 \times 14.7}$$

Before each run, the background leak rate (of the system without test samples) was also measured and subtracted from the actual test runs. To ensure a constant temperature, all leak tests were conducted at ~0.5-1 h after reaching the desired temperature (800 °C).

2.3 Thermal Cycling

The compressive mica seals were also evaluated for stability during thermal cycling. Thermal cycling was conducted between ~100 and 800 °C with a rapid (~20 °C/min) or a slow (~6 °C/min) heating rate and a slow cooling rate of ~2-3 °C/min. The samples were held at 800 °C for ~2 h before measuring the leak rates.

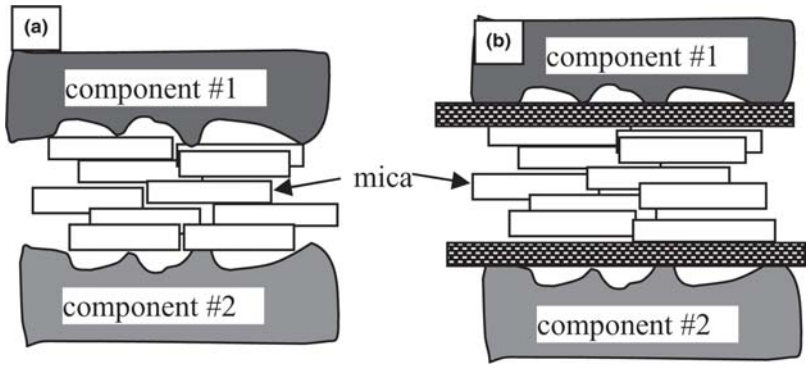

Fig. 3 Assembly of (a) conventional compressive mica seals pressed between two components and (b) "hybrid" mica seal where interlayers (shaded) are added at the two interfaces.

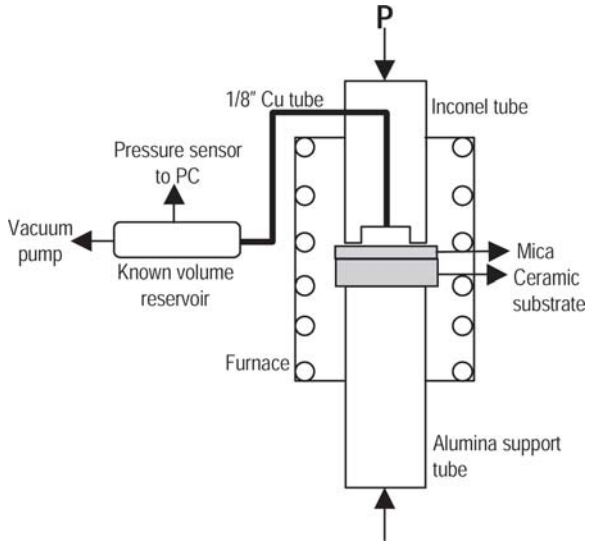

Fig. 4 Experimental setup for leak testing at elevated temperatures. Leak rates were determined by monitoring the pressure (vacuum or a positive pressure) versus time (Ref 8).

2.4 Mica Infiltration

Commercially available phlogopite mica paper was used to prepare "infiltrated" mica. The phlogopite mica had a thickness of ~75 μm and contained no binders. $Bi(NO_3)_3 \cdot 5H_2O$ (98%, Alfa Aesar, Ward Hill, MA) was chosen as the chemical for infiltration. Deionized water was used to make saturated bi-nitrate solutions. The infiltration was conducted by dispensing the solution onto the paper instead of immersing the mica paper into the solutions. The dried infiltrated micas were then evaluated in the hybrid form for thermal-cycle stability. They were pressed at 0.69 MPa between an IN600 fixture (50 × 50 mm) and a metal substrate of three materials: IN600, Haynes230, and SS430. The objective was to study the effect of CTE mismatch in these couples. The average CTE (from RT to 800 °C) values of these metals are ~17 ppm/°C (IN600), ~14.5 ppm/°C (Haynes230), and ~12.5 ppm/°C (SS430).

2.5 Open Circuit Voltage Test

To assess the sealing capability of the seals, open circuit voltage (OCV) tests were conducted using 50 × 50 mm sintered dense 8-YSZ plates. The sintered plates were machined flat to the desired size and thickness (~1 mm) and screen printed with silver paste on both sides. After electrode sintering, Pt wire leads were connected for the OCV tests. The dense 8-YSZ plate was pressed between an IN600 top cap (50 × 50 mm with a wall thickness of 5 mm) and an alumina bottom support. The hybrid mica seals were pressed between the 8-YSZ plate and the IN600 fixture at a stress of 0.69 MPa. A schematic drawing of the OCV test fixture and the mica seal arrangement is shown in Fig. 5. The OCV measurements were conducted at 800 °C after dwelling at temperature for about 1.5-2 h. A low hydrogen-content gas (2.55-2.71% H_2/balance Ar with ~3% H_2O) was used as the fuel with variable flow rates. Air was used as the oxidant on the cathode side with a flow rate of 100-200 sccm (standard cubic centimeter per minute).

3. Results and Discussion

3.1 Origin of Leak Path and Concept of "Hybrid" Mica Seals

For conventional compressive seals, a gasket material such as mica sheet was placed between two mating components (Fig. 3a) and a load was applied to achieve the seal. Potential advantages of a gasket seal include simplicity of design and fabrication and low cost. Viewing the microstructure of the mica gasket, either the monolithic single-crystal sheet or the mica paper of the discrete flakes (Fig. 3), one would expect to have two leak paths in conventional compressive mica seals: one at the interfaces between the mica paper and the mating components, and the other through the interstitials/flat voids between discrete mica flakes. Of these two types of leak paths, the interfaces between the mica paper and the mating components were suspected to be the major leak path, which was attributed to the surface roughness of the mating component or the mica paper. To verify this assumption, a simple test was conducted using a common glass slide for optical microscopy and an alumina integrated circuit (IC) substrate plate. The optical glass slide had no visible defects on its surface, and the thickness was uniform (Fig. 6a), and the alumina substrate had a surface roughness of <0.89 μm and shallow sintering voids on the surface (Fig. 6b). In the leak tests, the materials were pressed directly under a fine finished (#800 grit) Inconel pipe at various stresses. In addition, a third test of glass on glass was conducted by using a ring of an optical glass slide glued to the end of Inconel pipe and pressed against the optical glass slide.

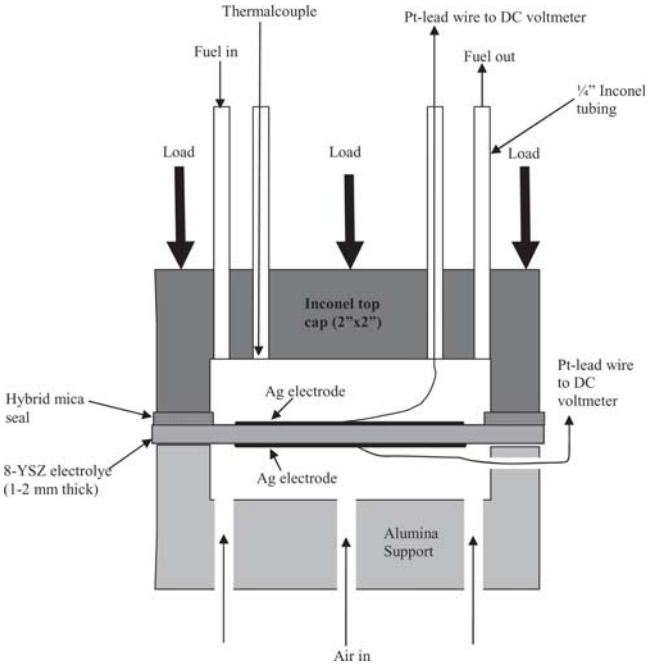

Fig. 5 Open circuit voltage test fixture (50 × 50 mm) is shown with a dense 8-YSZ plate and compressive mica seal on the fuel side. The pressing cap was made of IN600 with 4-6.35 mm IN600 tubes. The 8-YSZ plate was supported on an alumina block with three bottom holes for airflow.

The surface roughness at the interfaces of the three couples can be categorized qualitatively as low roughness, medium roughness, and high roughness for the glass/glass, Inconel/glass, and Inconel/alumina couples, respectively. The room-temperature leak rates of these three couples at various compressive stresses are plotted in Fig. 7. It is evident that the glass/glass couple in which the interface (leak path) was smoothest showed the lowest leak rates. The leak rates of the roughest interface (Inconel/alumina substrate) were the highest, and the leak rates of the medium roughness (Inconel/glass) were intermediate. The results clearly verify the surface roughness/defects effect on the leak rates for compressive seals.

After identifying the primary source of leaks, the hybrid mica seal concept was proposed. The hybrid mica seal contained a mica gasket as in the conventional compressive seal but also included compliant layers at the two interfaces (Fig. 3b). The compliant layer can be a glass, a glass-ceramic, or a metal in the form of thin sheet or foil, so a low-melting borosilicate glass (Ref 7), a Ba-Al-Ca silicate glass-ceramic (Ref 13), and a precious metal (Ag) as the interlayer (Ref 8) were tested. The results of the 800 °C leak rate tests of hybrid mica seals are shown in Fig. 8(a) for muscovite single-crystal sheet with the low-melting borosilicate glass interlayers, and Fig. 8(b) for the muscovite mica paper with Ag thin-foil interlayers. It was evident that the leak rates could be substantially reduced once these interfaces were sealed by the compliant metal or the wetting glass. It should be pointed out that these interlayer materials were not optimized but rather served to demonstrate proof of concept. For SOFC applications, these interlayer materials must also meet the stringent thermal and environmental long-term stability requirements; however, the close matching of CTEs may not be required.

3.2 Concept of "Infiltrated" Mica Seals

In the previous section and earlier work (Ref 7), it was found that the major leak paths for compressive mica seals were at the interfaces between the mica and the adjacent materials being sealed (metal or ceramics). Leak rates of the monolithic muscovite mica seals can be substantially reduced (2-3 orders of magnitude) by adding extra compliant layers (glass or metal foil) at these interfaces to form the so-called 'hybrid mica seals" (Ref 7, 8). However, the leak rates in these seals increased rapidly during initial thermal cycles. Further testing on phlogopite mica papers (in hybrid form) showed different behavior in terms of leak rate versus thermal cycling in that the leak rates gradually decreased with increasing of thermal cycles (Ref 12). From microstructural observations, it was found that some of the glass (from the compliant layers) had penetrated into the mica paper and resulted in leak rates that were insensitive to thermal cycles. Microstructural examination of the mica papers verified the presence of voids between the discrete mica flakes (Fig. 2d) that formed continuous 3-D leak paths through the mica paper. The concept of 'infiltrated" mica was therefore proposed. The objective was to introduce a wetting or glass-forming material into the voids between mica flakes such that the continuous 3-D leak paths could be reduced to 2-D geometry (Fig. 9), thereby reducing the leak rate through the material. It was expected that the flatter the fracture surfaces (leak paths), the closer the geometrical match when they were compressed against each other. This would result in narrower gaps between the fracture planes and lead to lower leak rates and less damage upon thermal cycling. The concept of the infiltrated micas is illustrated in Fig. 9, where the infiltrated materials will wet or form necks at the voids and form a controlled 2-D leak path upon thermal cycling (dotted line in Fig. 9) (Ref 14).

3.3 Effect of CTE Mismatch on the Thermal Cycle Stability of "Infiltrated" Micas

The infiltrated mica was tested successfully with H_3BO_3 as the chemical for infiltration (Ref 14). The concept was further tested to evaluate the tolerance in CTE mismatches on high-temperature leak rates during thermal cycling using bismuth nitrate as the infiltrant. The CTE mismatches were selected using three typical metals: IN600, Haynes230, and SS430. The average CTEs (from RT to 800 °C) for these three metals are ~17, ~15, and ~12.5 ppm/°C, respectively. The CTE of phlogopite mica is ~11 ppm/°C (along the basal plane). IN600 and Haynes230 are superalloys with superior high-temperature oxidation resistance and mechanical properties. However, because of their high CTEs, they can only be considered as SOFC interconnect candidates if compliant seals (such as mica seals) are used. SS430 has a close CTE match with the typical anode-supported cells but suffers severe oxidation at elevated temperatures. Tests of the infiltrated micas in these three metal couples, therefore, covered a wide range of CTE mismatch over which other sealing approaches (e.g., glass and braze) are not likely to be suitable.

The leak rates versus thermal cycling of the Bi-nitrate infiltrated mica in the three metal couples are shown in Fig. 10. It is interesting to note that the leak rates are much lower for all three metal couples, i.e., less than 4×10^{-3} sccm/cm, than for the as-received mica [$(2\text{-}3) \times 10^{-2}$ sccm/cm]. Leak rates of the Bi-nitrate infiltrated mica appeared to be independent of the wide range of CTE mismatches among the three metal couples.

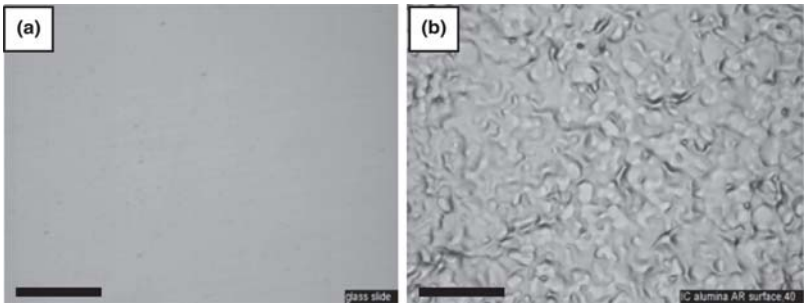

Fig. 6 Surface morphology of (a) the optical glass side and (b) the alumina IC substrate (bars are 100 μm).

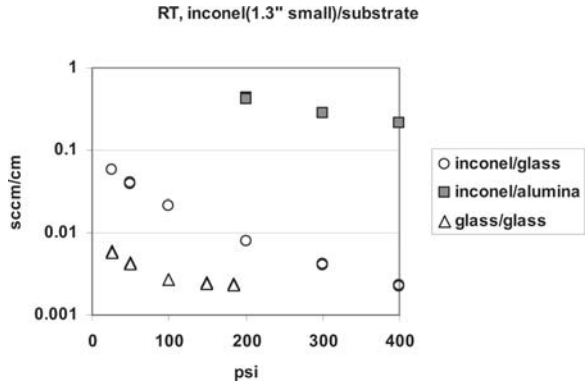

Fig. 7 Effect of surface roughness/defects on the room-temperature leak rates of three test couples at various stresses

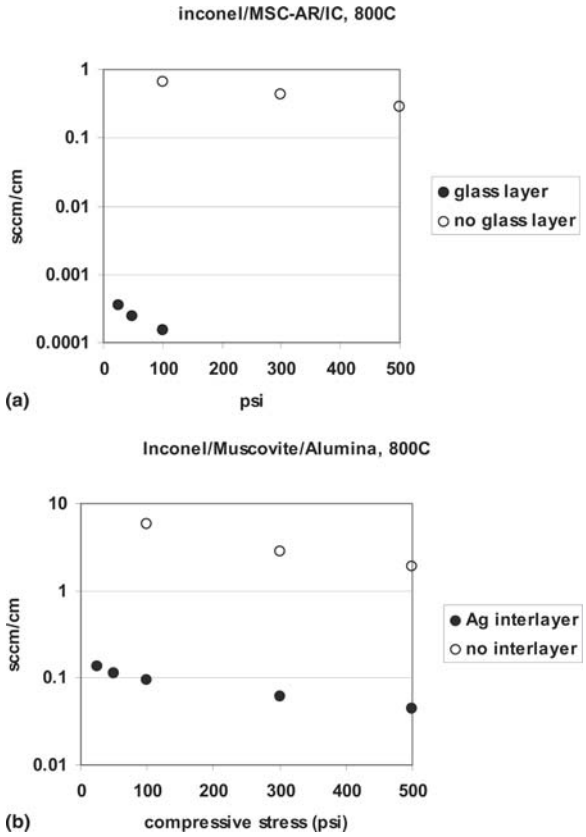

Fig. 8 Leak rates at 800 °C of hybrid mica seals with different interlayers: (a) muscovite single-crystal sheet with the low-melting borosilicate glass (Ref 7), and (b) muscovite mica paper with thin Ag foils (Ref 8)

In addition, the leak rates were rather insensitive to the number of thermal cycles (the fluctuation of leak rates during the 36 cycles is likely caused by ambient temperature fluctuations). Compared with the H_3BO_3-infiltrated micas (Ref 14), the Bi-nitrate infiltrated micas showed low leak rates in the first cycle instead of a gradual decrease with thermal cycles. This behavior is likely due to the presence of excess Bi-nitrate on the mica surfaces as well as the thinner mica used (75 μm) as compared with the H_3BO_3-infiltrated mica (100 μm). It was found that Bi-nitrate [$Bi(NO_3)_3 \cdot 5H_2O$] did not form a stable aqueous solution but instead decomposed to form $BiONO_3 \cdot H_2O$ white precipitates. After infiltration and drying, a coating of the precipitate remained on the mica discs. In post-cycling microstructural characterization, it was also found that the mica could be easily detached from the test fixtures. The penetration of Bi_2O_3 into the mica paper and the smooth fracture surface of the cleaved mica were evident with scanning electron microscopy. It needs to be noted that these chemicals (e.g., bismuth nitrate, which yields bismuth oxide at higher temperatures) are not stable in actual SOFC environments. However, they were considered to be appropriate choices for these proof-of-concept experiments.

3.4 Open Circuit Voltage Test During Long-Term Cycling

A low-hydrogen fuel (2.55-2.71% H_2/balance Ar) was chosen for the long-term OCV and thermal-cycling tests. The use of a dilute hydrogen fuel allowed for establishment of reducing conditions typical of the anode side of a SOFC with no risk of fire or explosion during the seal tests. The equilibrium oxygen partial pressure at 800 °C was calculated to be 6.45×10^{-19} atm for a 2.71% H_2/Ar fuel (with 3% H_2O) and 4.2×10^{-22} atm for pure hydrogen fuel (97% H_2/3% H_2O). It is evident that the use of a low-hydrogen fuel still provided a very reducing environment. The theoretical (Nernst) voltage for the dilute hydrogen fuel versus air across the 8-YSZ electrolyte is 0.934 V.

In addition to providing sufficiently reducing conditions in a safe manner, the dilute hydrogen also offered higher sensitivity to leaks during the OCV tests. In these tests, a mica seal was applied only on the anode side of the YSZ plate and then compressed with the IN600 fixture (Fig. 5). The cathode side of the YSZ plate was directly pressed against the alumina support block without any seals in between. The alumina support block had several holes underneath for airflow. The gas pressure at the anode side was maintained slightly higher than the ambient (~102.7 kPa) by using a downstream gas bubbler filled with ~13 cm of water. Any leaked fuel would have a minimum

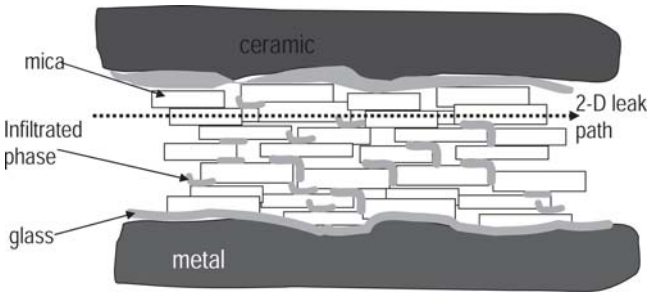

Fig. 9 Concept of the "infiltrated" mica seals. Infiltrated phases will fill in the voids and form necks with mica flakes, such that the original 3-D leak path will be reduced to 2-D leak path (dotted line) (Ref 14).

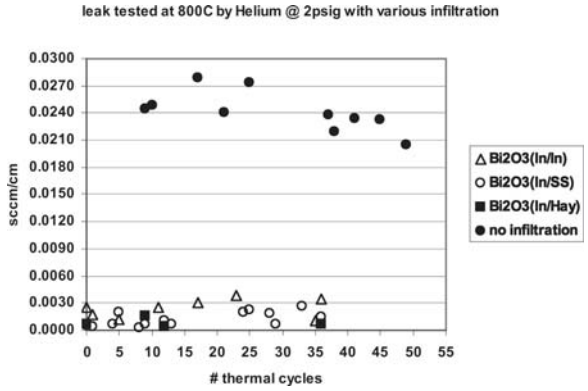

Fig. 10 Effect of CTE mismatch on the thermal cycle stability of infiltrated phlogopite micas. Mica in hybrid form was pressed between three metal couples of different CTE mismatch.

effect on the cathode side because it would immediately react with the air in the furnace chamber. On the other hand, any air (21% O_2) leaks into the anode chamber should have a more pronounced effect on the equilibrium oxygen partial pressure for the low-hydrogen (e.g., 2.71% H_2/Ar) fuel compared with a pure hydrogen fuel (e.g., 100% H_2).

In the OCV tests, the fuel flow rate was fixed at 63 sccm. This flow rate would correspond to an 80% fuel utilization for a cell with an active area of 10 cm^2 operating at a current density of 0.75 A/cm^2 on pure hydrogen (i.e., 97% H_2 + ~3% H_2O). The OCV versus number of thermal cycles for the 50 × 50 mm 8-YSZ electrolyte plate with the hybrid phlogopite mica-paper seal pressed at 0.69 MPa is shown in Fig. 11. This sample survived 1026 thermal cycles when thermally cycled between 100 and 800 °C at a rapid heating rate of 20 °C/min. The initial (the first time reaching 800 °C) OCV was 0.934 V, exactly matching with the theoretical (Nernst) voltage for 2.71% H_2/balance Ar with 3% H_2O versus air at 800 °C. As the thermal cycles continued, the OCV decreased to about 0.92 V in the initial ~50 thermal cycles, after which the OCV stabilized for the subsequent thermal cycles at 0.919 V ± 2 mV, which is only 1.7% lower than the Nernst voltage. The drop of OCV in the initial thermal cycles is likely caused by mica fracture (cleavage) associated with these cycles (Ref 11). For hybrid mica seals, the glass interlayers will bond strongly to the mating materials (IN600 and 8-YSZ in the current study) and to the top several layers of the mica (the final thickness of the glass layer was ~10 μm; no spalling was observed during thermal cycling even though the CTE mismatch was large at the IN600 side). During initial thermal cycling, the large CTE mismatch between the IN600 fixture, the mica paper, and the 8-YSZ electrolyte plate may form new fractures (leak paths) between the mechanically interlocked flakes in the mica paper. Fortunately, after a few dozen thermal cycles, the formation of additional leak paths apparently ceased, as the OCV remained fairly constant. Postcycling analysis showed typical wear particle formation at the fracture surface (Fig. 12A), consistent with earlier report that the frictional wear damages were localized to that specific fracture plane (Ref 10). The micas below the fracture plane showed no wear damage at all (Fig. 12B). The microstructure of the intact micas also suggested some thermal stability of the phlogopite mica in the simulated reducing and moist environments because the mica was exposed to the environments for a total of 2052 h at 800 °C. Overall, the hybrid seals demonstrated the desired long-term thermal cycle stability.

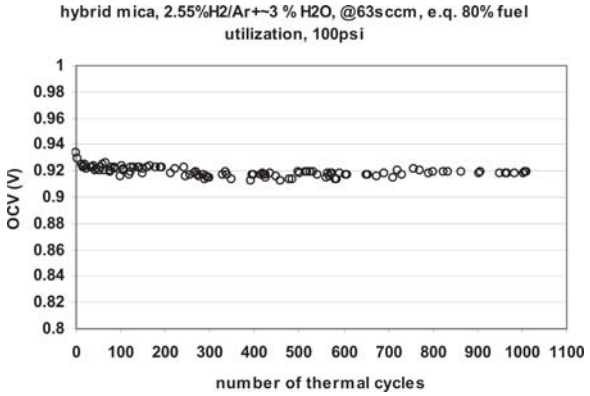

Fig. 11 OCV versus thermal cycles for the 50 × 50 mm 8-YSZ with hybrid mica seal pressed at 0.69 MPa. The fuel was 2.55-2.71% H_2/Ar + ~3% H_2O at a flow rate of 63 sccm, equivalent to 80% fuel utilization by a 10 cm^2 cell operating at a current density of 0.75 A/cm^2.

3.5 Combined Aging and Thermal Cycling

As mentioned earlier, the SOFC sealants need to demonstrate not only thermal-cycle stability but also thermal, chemical, and mechanical stability during long-term (>40,000 h) operation. Several combined aging and thermal cycling tests of the hybrid phlogopite mica seals have been conducted. These tests were conducted by aging at 800 °C in a flowing reducing (~2.5-2.7% H_2/Ar + ~3% H_2O) environment for ~1000 h followed by short (~30 cycles) thermal cycling between 100 and 800 °C. The mica was pressed between an IN600 fixture and 8YSZ electrolyte plate (50 × 50 mm) at a very low stress of 41.4 kPa. The 800 °C leak rate versus aging time is shown in Fig. 13. The initial leak rates were ~0.02 sccm/cm and gradually decreased to ~0.002-0.003 sccm/cm at ~600 h. The leak rates then increased rapidly after aging ~800 h to ~0.05 sccm/cm. After aging for 1036 h, thermal cycling was initiated between ~100 and 800 °C. The leak rates were ~0.08 sccm/cm at the 5th cycle, ~0.1 sccm/cm at the 15th cycle, and ~0.3 sccm/cm at the 21st cycle. Such high leak rates were equivalent to the leak rate through rigid glass seals after fracture caused by CTE mismatch.

Postcycling analysis showed that the high leak rates were related to the reaction of the phlogopite mica with the glass

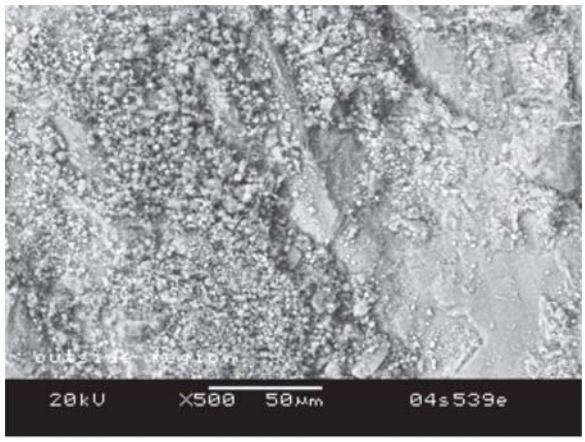

(a)

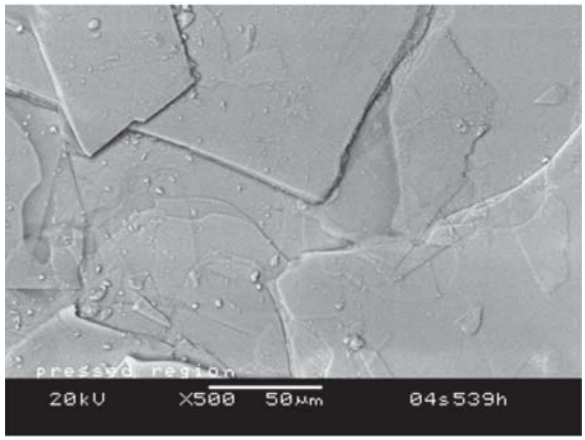

(b)

Fig. 12 Scanning electron microscopy shows the surface morphology of the hybrid phlogopite mica after 1026 thermal cycles in the long-term OCV and cycling test: (a) fracture surface of the mica at the interface and (b) mica from layers below the fracture surface.

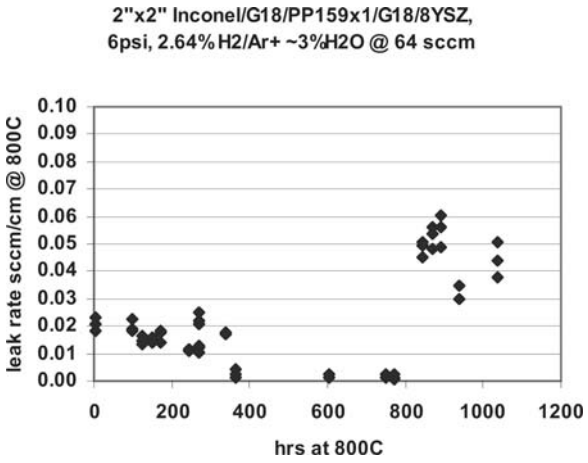

Fig. 13 Combined aging and thermal cycling test of hybrid phlogopite mica seal pressed between an IN600 fixture (50 × 50 mm) and an YSZ electrolyte plate at 800 °C. The sample was pressed at low stress of 41.4 kPa and flowing with 64 sccm of ~2.5-2.7% H_2/Ar + ~3% H_2O.

Fig. 14 Typical fracture surface of the hybrid phlogopite mica after aging at 800 °C for 1036 h followed by 21 thermal cycles between ~100 and 800 °C in a flowing reducing and wet environment. The rough surface indicated the phlogopite mica reacted completely with the Ba-Al-Ca silicate glass layer and fractured along the Inconel 600 interface due to large CTE mismatch.

layers. It was found that the phlogopite mica completely reacted with the Ba-Al-Ca silicate glass interlayers (which also contained B_2O_3 to improve wetting at ~830-850 °C) (Ref 13). The fracture surface therefore showed no smooth cleavage planes of mica but instead the rough morphology of the crystallized and reacted glass-ceramic (Fig. 14). The presence of Mg and K also confirmed the reaction of the glass with the phlogopite mica ($KMg_3(AlSi_3O_{10})(OH,F)_2$), as shown in Fig. 15(a), as compared with the Ba-Al-Ca silicate glass alone (Fig. 15b). It is interesting to also note the presence of Cr at the fracture surface (Fig. 15a) that likely comes from the IN600. The cause for the severe reaction of hybrid phlogopite mica through the whole thickness (~100 μm) during the aging test is not yet fully understood. It is not clear why the long-term OCV and cycling-tested phlogopite mica showed only limited degradation of the mica at the fracture planes (Fig. 12) after a total holding time of 2052 h at 800 °C, whereas the mica seal aged continuously for 1036 h in the same environment showed reaction through the entire mica thickness (Fig. 14).

4. Summary and Conclusion

A comprehensive study of mica-based compressive seals for SOFC was reported. It was found that the major leak paths in conventional mica seals were at the sealing interfaces, not through the mica itself. By introducing extra compliant or wetting layers at these interfaces, the high-temperature leak rates could be substantially reduced. The leak rates could be further reduced by about 10 times when the micas were infiltrated with a wetting agent. The infiltrated micas also showed excellent thermal-cycle stability with wide tolerance of CTE mismatches. Very-long thermal cycling, up to 1026 cycles, was conducted on a hybrid phlogopite mica. OCV test showed minimal (~1.7%) reduction of voltage from the Nernst voltage. Microstructural characterization also revealed that frictional wear damage was localized rather than extending through the mica thickness. However, further testing on combined aging and thermal cycling of hybrid micas showed severe reaction of mica with glass interlayers, and future modification of the glass interlayers will be required. Overall, the hybrid mica seal has demonstrated low leak rates and good thermal cycle stability over a wide range of CTE mismatch.

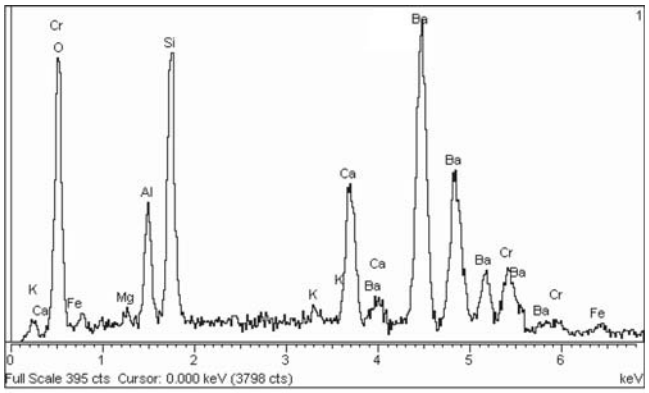

(a)

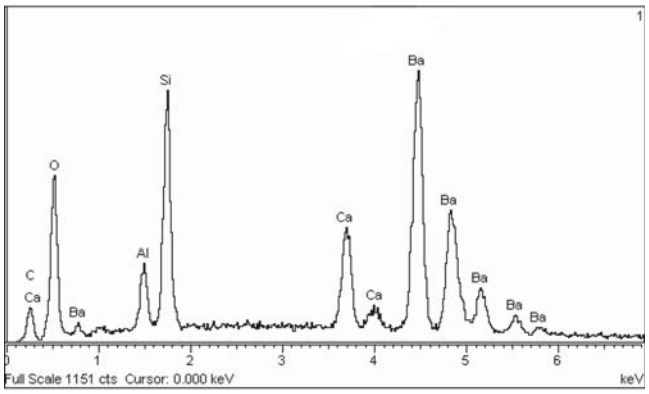

(b)

Fig. 15 (a) EDS of the fracture surface of Fig. 13; (b) EDS of the Ba-Al-Ca silicate glass

Acknowledgments

The authors thank S. Carlson for SEM sample preparation and J. Coleman for SEM analysis. This paper was funded as part of the Solid-State Energy Conversion Alliance (SECA) Core Technology Program by the U.S. Department of Energy National Energy Technology Laboratory (NETL). Pacific Northwest National Laboratory is operated by Battelle Memorial Institute for the U.S. Department of Energy under Contract no. DE-AC06-76RLO 1830.

References

1. T. Yamamoto, H. Itoh, M. Mori, N. Mori, and T. Watanabe, Compatibility of Mica Glass-Ceramics as Gas-Sealing Materials for SOFC, *Denki Kagaku,* 1996, **64,** p 575-581
2. K. Ley, M. Krumpelt, J. Meiser, and I. Bloom, Glass-Ceramic Sealants for Solid Oxide Fuel Cells: Part I. Physical Properties, *J. Mater. Res.,* 1996, **11,** p 1489-1493
3. P. Larsen, C. Bagger, M. Morgensen, and J. Larsen, *Solid Oxide Fuel Cells-IV,* PV 95-1, M. Dokiya, O. Yamamoto, H. Tagawa, and S. Singhal, Ed., Vol. 69, Electrochemical Society, 1995
4. N. Lahl, D. Bahadur, K. Singh, L. Singheiser, and K. Hilpert, Chemical Interactions between Aluminosilicate Base Sealants and the Components on the Anode Side of Solid Oxide Fuel Cells, *J. Electrochem. Soc.,* 2002, **149,** p A607-A614
5. K.S. Weil, J.S. Hardy, and J.Y. Kim, Use of a Novel Ceramic-to-Metal Braze for Joining in High Temperature Electrochemical Devices, *Joining of Advanced and Specialty Materials V,* American Society of Metals, 2002
6. K.S. Weil, J.S. Hardy, and J.Y. Kim, Development of a Silver-Copper Oxide Braze for Joining Metallic and Ceramic Components in Electrochemical Devices, *Proc. of the Int. Brazing and Soldering 2003 Conf.,* American Welding Society, 2003
7. Y.-S. Chou, J.W. Stevenson, and L.A. Chick, Ultra-Low Leak Rate of Hybrid Compressive Mica Seals for Solid Oxide Fuel Cells, *J. Power Sources,* 2002, **112,** p 130-136
8. Y.-S. Chou, J.W. Stevenson, and L.A. Chick, Novel Compressive Mica Seals with Metallic Interlayers for Solid Oxide Fuel Cell Applications, *J. Am. Ceram. Soc,* 2003, **86,** p 1003-1007
9. S.P. Simner and J.W. Stevenson, Compressive Mica Seals for SOFC Applications, *J. Power Sources,* 2001, **102,** p 310-316
10. Y.-S. Chou and J.W. Stevenson, Mid-term Stability of Novel Mica-Based Compressive Seals for Solid Oxide Fuel Cells, *J. Power Sources,* 2003, **115,** p 274-278
11. Y.-S. Chou and J.W. Stevenson, Thermal Cycling and Degradation Mechanisms of Compressive Mica-Based Seals for Solid Oxide Fuel Cells, *J. Power Sources,* 2002, **112,** p 376-383
12. Y.-S. Chou and J.W. Stevenson, Phlogopite Mica-Based Compressive Seals for Solid Oxide Fuel Cells: Effect of Mica Thickness, *J. Power Sources,* 2002, **124,** p 473-478
13. K. Meinhardt and L. Pederson, U.S. Patent 6 430 966
14. Y.-S. Chou and J.W. Stevenson, Novel Infiltrated Phlogopite Mica Compressive Seals for Solid Oxide Fuel Cells, *J. Power Sources,* 2004, **135,** p 72-78